



Provided by the author(s) and University College Dublin Library in accordance with publisher policies. Please cite the published version when available.

| | |
|-------------------------------------|---|
| Title | A Class-F CMOS Oscillator |
| Authors(s) | Babaie, Masoud; Staszewski, Robert Bogdan |
| Publication date | 2013-08-07 |
| Publication information | IEEE Journal of Solid-State Circuits, 48 (12): 3120-3133 |
| Publisher | IEEE |
| Item record/more information | http://hdl.handle.net/10197/8419 |
| Publisher's statement | © 2013 IEEE. Personal use of this material is permitted. Permission from IEEE must be obtained for all other uses, in any current or future media, including reprinting/republishing this material for advertising or promotional purposes, creating new collective works, for resale or redistribution to servers or lists, or reuse of any copyrighted component of this work in other works. |
| Publisher's version (DOI) | 10.1109/JSSC.2013.2273823 |

Downloaded 2022-08-25T18:56:35Z

The UCD community has made this article openly available. Please share how this access benefits you. Your story matters! (@ucd_oa)



A Class-F CMOS Oscillator

Masoud Babaie, *Student Member, IEEE*, and Robert Bogdan Staszewski, *Fellow, IEEE*

Abstract—An oscillator topology demonstrating an improved phase noise performance is proposed in this paper. It exploits the time-variant phase noise model with insights into the phase noise conversion mechanisms. The proposed oscillator is based on enforcing a pseudo-square voltage waveform around the LC tank by increasing the third-harmonic of the fundamental oscillation voltage through an additional impedance peak. This auxiliary impedance peak is realized by a transformer with moderately coupled resonating windings. As a result, the effective impulse sensitivity function (ISF) decreases thus reducing the oscillator's effective noise factor such that a significant improvement in the oscillator phase noise and power efficiency are achieved. A comprehensive study of circuit-to-phase-noise conversion mechanisms of different oscillators' structures shows the proposed class-F exhibits the lowest phase noise at the same tank's quality factor and supply voltage. The prototype of the class-F oscillator is implemented in TSMC 65-nm standard CMOS. It exhibits average phase noise of -136 dBc/Hz at 3 MHz offset from the carrier over 5.9–7.6 GHz tuning range with figure-of-merit of 192 dBc/Hz. The oscillator occupies 0.12 mm² while drawing 12 mA from 1.25 V supply.

Index Terms—Class-F oscillator, impulse sensitivity function, phase noise, digitally controlled oscillator, VCO, transformer.

I. INTRODUCTION

DESIGNING voltage-controlled and digitally-controlled oscillators (VCO, DCO) of high spectral purity and low power consumption is quite challenging, especially for GSM transmitter (TX), where the oscillator phase noise must be less than -162 dBc/Hz at 20 MHz offset frequency from 915 MHz carrier [1]. At the same time, the RF oscillator consumes disproportionate amount of power of an RF frequency synthesizer [2], [3] and burns more than 30% of the cellular RX power [4], [5]. Consequently, any power reduction of RF oscillators will greatly benefit the overall transceiver power efficiency and ultimately the battery lifetime. This motivation has encouraged an intensive research to improve the power efficiency of an RF oscillator while satisfying the strict phase noise requirements of the cellular standards.

The traditional class-B oscillator (Fig. 1(a)) is the most prevalent architecture due its simplicity and robustness. However, its phase noise and power efficiency performance drops dramatically just by replacing the ideal current source with a real one. Indeed, the traditional oscillator reaches its best performance for the oscillation amplitude of near supply voltage V

TABLE I
NORMALIZED ZERO-CROSSING SLOPE OF THE PROPOSED OSCILLATOR

| | Normalized zero-crossing slope |
|---------------------------|---|
| Traditional LC | 1 |
| Proposed tank (primary) | $1+3\zeta = 1+3\cdot 1/6 = 1.5$ |
| Proposed tank (secondary) | $G_1-3G_2\zeta = 2.1 - 3\cdot 0.4\cdot 1/6 = 1.9$ |

D. Proposed Class-F Oscillator

The desired tank impedance, inductance and capacitance ratios were determined above to enforce the pseudo-square-wave oscillation voltage around the tank. Now, two transistors should be customarily added to the transformer-based resonator to sustain the oscillation. There are two options, however, as shown in Fig. 10, for connecting the transformer to the active gm-devices. The first option is a transformer-coupled class-F oscillator in which the secondary winding is connected to the gate of the gm-devices. The second option is a cross-coupled class-F oscillator with a floating secondary transformer winding, which only physically connects to tuning capacitors C_2 . The oscillation voltage swing, the equivalent resonator quality factor and tank input impedance are the same for both options. However, the gm-device sustains larger voltage swing in the first option. Consequently, its commutation time is shorter and the active device noise factor is lower. In addition, the gm-device generates higher amount of the 3rd harmonic, which results in sharper pseudo-square oscillation voltage with lower ISF rms value. The second major difference is about the possibility of oscillation at ω_2 instead of ω_1 . The root-locus plot in Fig. 11 illustrates the route of pole movements towards zeros for different values of the oscillator loop trans-conductance gain (G_m). As can be seen in Fig. 11(b), both resonant frequencies (ω_1, ω_2) can be excited simultaneously with a relatively high value of G_m for the cross-coupled class-F oscillator of Fig. 10(b). It can increase the likelihood of the undesired oscillation at ω_2 . However, the transformer-coupled circuit of Fig. 10(a) demonstrates a different behavior. The lower frequency conjugate pole pair moves into the right-hand plane by increasing the absolute value of G_m , while the higher poles are pushed far away from imaginary axis (see Fig. 11(a)). This guarantees the oscillation can only happen at ω_1 . Consequently, it becomes clear that the transformer-coupled oscillator is a better option due to its phase noise performance and the guaranty of operation at the right resonant frequency. Nevertheless, the gate parasitic capacitance appears at the drain through a scaling factor of n^2 , which reduces its tuning range somewhat as compared to the cross-coupled candidate.

Fig. 12 illustrates the unconventional oscillation voltage waveforms of the proposed transformer-coupled class-F oscillator. As specified in Section II.C, the 3rd harmonic component of the drain voltage attenuates at the gate and thus a sinusoidal wave is seen there. The gate-drain voltage swing goes as high as $2.7 \cdot V_{DD}$ due to the significant voltage gain of the tank. Hence, using thick oxide gm-devices is a constraint to satisfy the time-dependent dielectric breakdown (TDDB) issue for less than 0.01% failure rate during ten years of the oscillator operation [20], [21]. The costs are larger parasitic capacitance and slightly lower frequency tuning range.

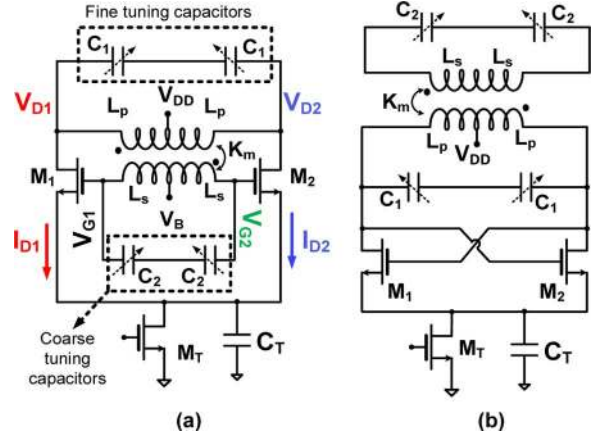


Fig. 10. Two options of the transformer-based class-F oscillator: (a) transformer-coupled; and (b) cross-coupled. The first option was chosen as more advantageous in this work.

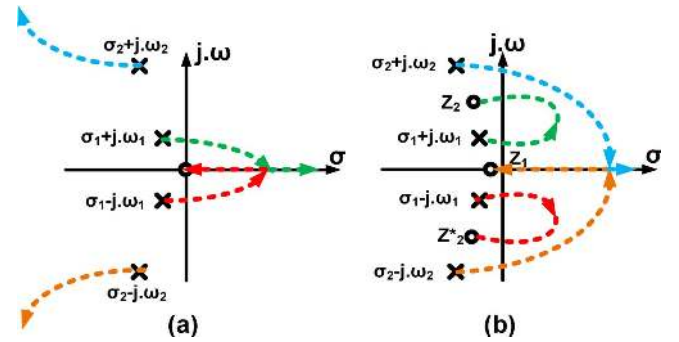


Fig. 11. Root-locus plot of the transformer-based class-F oscillator: (a) transformer-coupled structure of Fig. 10(a); and (b) cross-coupled structure of Fig. 10(b).

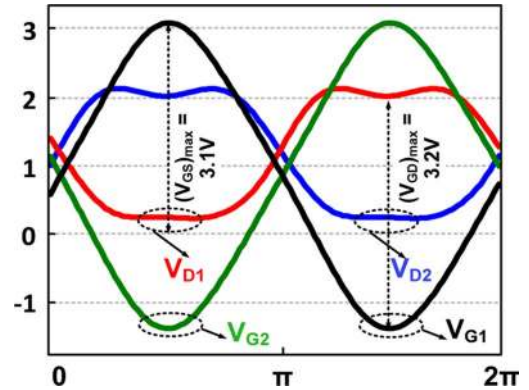


Fig. 12. Oscillation voltage waveforms of class-F oscillator.

The frequency tuning requires a bit different consideration in the class-F oscillator. Both C_1 and C_2 must, at a coarse level, be changed simultaneously to maintain $L_s C_2 / L_p C_1$ ratio such that ω_2 aligns with $3\omega_1$.

Fig. 13 shows the transient response of the class-F oscillator. At power up, the oscillation voltage is very small and the drain current pulses have narrow and tall shape. Even though the tank has an additional impedance at $3\omega_1$, the 3rd harmonic component of the drain current is negligible and, consequently, the drain oscillation resembles a sinusoid. At steady state, gate oscillation voltage swing is large and the gm-device drain current is square-wave. Consequently, the combination of the tank input

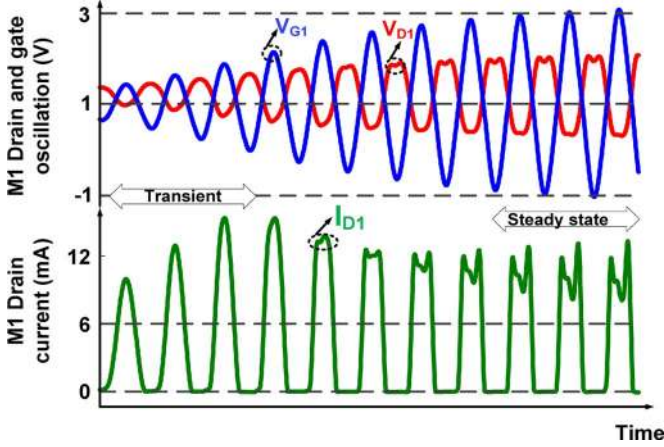


Fig. 13. Transient response of the class-F oscillator.

impedance with significant 3rd harmonic component of drain current results in the pseudo-square wave for the drain oscillation voltage. This justifies its “class-F” designation.

III. CLASS-F PHASE NOISE PERFORMANCE

A. Quality Factor of Transformer-Based Resonator

The Q-factor of the complex tank, which comprises two coupled resonators, does not appear to be as straightforward in intuitive understanding as the Q-factor of the individual physical inductors. It is, therefore, imperative to understand the relationship between the open-loop Q-factor of the tank versus the Q-factor of the inductive and capacitive parts of the resonator.

First, suppose the tuning capacitance losses are negligible. Consequently, the oscillator equivalent Q-factor just includes the tank’s inductive part losses. The open-loop Q-factor of the oscillator is defined as $\omega_0/2 \cdot d\phi/d\omega$, where ω_0 is the resonant frequency and $d\phi/d\omega$ denotes the slope of the phase of the oscillator open-loop transfer function [22]. To determine the open-loop Q, we need to break the oscillator loop at the gate of M_1 , as shown in Fig. 14. The open-loop transfer function is thus given by

$$H(s) = \frac{V_{\text{out}}}{I_{\text{in}}} = \frac{Ms}{As^4 + Bs^3 + Cs^2 + Ds + 1} \quad (18)$$

where, $A = (L_p L_s C_1 C_2 (1 - k_m^2))$, $B = (C_1 C_2 (L_s r_p + L_p r_s))$, $C = (L_p C_1 + L_s C_2 + r_p r_s C_1 C_2)$, and $D = (r_p C_1 + r_s C_2)$. After carrying out lengthy algebra and considering $(1 - C\omega^2 + A\omega^4 \approx 0)$ at the resonant frequencies,

$$Q_i = -\frac{\omega}{2} \frac{d\phi(\omega)}{d\omega} = \frac{(C\omega - 2A\omega^3)}{(D - B\omega^2)} \quad (19)$$

Substituting A, B, C and D into (19), then swapping r_p and r_s with $L_p\omega/Q_p$ and $L_s\omega/Q_s$, respectively, and assuming $Q_p Q_s \gg 1$, we obtain

$$Q_i = \frac{(L_p C_1 + L_s C_2) - 2(L_p L_s C_1 C_2 (1 - k_m^2)) \omega^2}{\left(\frac{L_p C_1}{Q_p} + \frac{L_s C_2}{Q_s}\right) - \left(C_1 C_2 L_s L_p \left(\frac{1}{Q_p} + \frac{1}{Q_s}\right)\right) \omega^2} \quad (20)$$

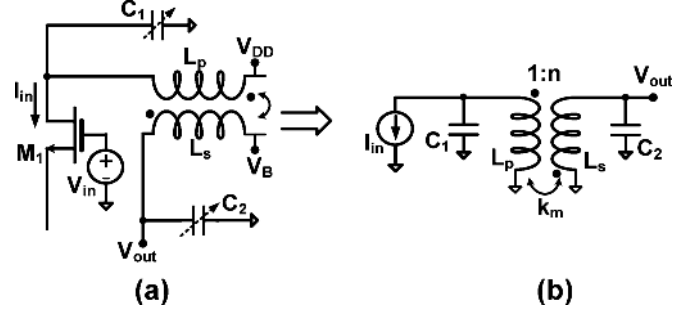


Fig. 14. Open-loop circuit for unloaded Q-factor calculation (a); its equivalent circuit (b).

Substituting (5) as ω into the above equation and carrying out the mathematics, the tank’s inductive part Q-factor at the main resonance is

$$Q_i = \frac{(1 + X^2 + 2k_m X)}{\left(\frac{1}{Q_p} + \frac{X^2}{Q_s}\right)} \quad (21)$$

To help with an intuitive understanding, let us consider a boundary case. Suppose, that C_2 is negligible. Therefore, X-factor is zero and (21) predicts that the Q_i equals to Q_p . This is not surprising, because no energy would be stored at the transformer’s secondary winding and its Q-factor would not have any contribution to the equivalent Q-factor of the tank. In addition, (21) predicts that the equivalent Q-factor of the tank’s inductive part can exceed Q-factors of the individual inductors. To the authors’ best knowledge, this is the first ever report of quantifying the equivalent Q-factor of the transformer-based resonator at its resonant frequency in a general case that clearly proves Q-factor enhancement over that of the transformer’s individual inductors. The maximum tank’s inductive part Q-factor is obtained at the following X-factor for a given k_m , Q_p and Q_s .

$$X_{Q_{\text{max}}} = \frac{Q_s}{Q_p} \quad (22)$$

For a typical case of $Q_s = Q_p = Q_0$, the maximum Q_i at ω_1 is calculated by

$$\begin{cases} X_{Q_{i,\text{max}}} = 1 \\ Q_{i,\text{max}} = Q_0(1 + k_m) \end{cases} \quad (23)$$

The above equation indicates that the equivalent Q-factor of the inductive part of the transformer-based resonator can be enhanced by a factor of $1 + k_m$ at the optimum state. However, it does not necessarily mean the Q-factor of the transformer-based tank generally is superior to the simple LC resonator. The reason is that it is not possible to optimize the Q-factor of both windings of a 1:n transformer at a given frequency and one needs to use lower metal layers for the transformer cross connections, which results in more losses and lower Q-factor [23], [24]. For this prototype, the X-factor is around 3 with $k_m = 0.7$ and the simulated Q_p and Q_s are 14 and 20 respectively. Based on (21), the equivalent Q-factor of the inductive part of the tank would be about 26, which is higher than that of the transformers’ individual inductors.

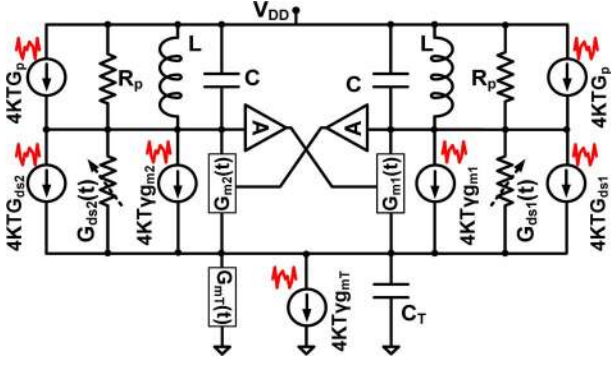


Fig. 15. RF CMOS oscillator noise sources.

The Q-factor of the switched capacitance largely depends on the tuning range (TR) and operating frequency of the oscillator and is about 42 for the TR of 25% at 7 GHz resulting in an average Q-factor of 16 for the tank in this design.

B. Phase Noise Mechanism in Class-F Oscillator

According to the linear time-variant model [13], the phase noise of the oscillator at an offset frequency $\Delta\omega$ from its fundamental frequency is expressed as,

$$L(\Delta\omega) = 10 \log_{10} \left(\frac{\sum_i N_{L,i}}{2q_{\max}^2 (\Delta\omega)^2} \right) \quad (24)$$

where, q_{\max} is the maximum charge displacement across the tuning capacitor C, and $N_{L,i}$ is the effective noise produced by i th device given by

$$N_{L,i} = \frac{1}{2\pi N^2} \int_0^{2\pi} \Gamma_i^2(t) \overline{i_{n,i}^2(t)} dt \quad (25)$$

where $\overline{i_{n,i}^2(t)}$ is the white current noise power density of the i th noise source, Γ_i is its relevant ISF function from the corresponding i th device noise, and N is the number of resonators in the oscillator. N is considered one for single-ended and two for differential oscillator topologies with a single LC tank [7].

Fig. 15 illustrates the major noise sources of CMOS class-B, C and F oscillators. R_p and $G_{ds1,2}(t)$ represent the equivalent tank parallel resistance and channel conductance of the gm transistors, respectively. On the other hand, $G_{m1,2}$ and G_{mT} model the noise due to transconductance gain of active core and current source transistors, respectively. By substituting (25) into (24) and carrying out algebra, the phase noise equation is simplified to

$$L(\Delta\omega) = 10 \log_{10} \left(\frac{K_B T R_p}{2Q_t^2 V_p^2} \cdot F \cdot \left(\frac{\omega_0}{\Delta\omega} \right)^2 \right) \quad (26)$$

where Q_t is the tank's equivalent quality factor and V_p is the maximum oscillation voltage amplitude, derived by

$$V_p = \begin{cases} \left(\frac{1}{3} + \zeta \right) \sqrt{\left(1 + \frac{1}{3\zeta} \right)} \cdot \alpha_I \cdot R_p \cdot I_B, & \frac{1}{9} \leq \zeta \leq 1 \\ (1 - \zeta) \cdot \alpha_I \cdot R_p \cdot I_B, & 0 \leq \zeta \leq \frac{1}{9} \end{cases} \quad (27)$$

where α_I is the current conversion efficiency of the oscillator, expressed as the ratio of the fundamental component of gm-devices drain current to dc current I_B of the oscillator. F in (26) is the effective noise factor of the oscillator, expressed by

$$F = \sum_i \frac{1}{2\pi} \int_0^{2\pi} \Gamma_i^2(t) \frac{\overline{i_{n,i}^2(t)} R_p}{4K_B T} dt \quad (28)$$

Suppose that C_T is large enough to filter out the thermal noise of the tail transistor. Consequently, F consists of the noise factor of the tank (F_{tank}), transistor channel conductance (F_{GDS}) and gm of core devices (F_{GM}). The expressions of F_{tank} and F_{GDS} are

$$F_{\text{Tank}} = \frac{1}{\pi} \int_0^{2\pi} \Gamma_{\text{tank}}^2(t) dt = 2\Gamma_{\text{rms}}^2 \approx \frac{1 + 9\zeta^2}{(1 + 3\zeta)^2} \quad (29)$$

$$F_{GDS} = \frac{1}{\pi} \int_0^{2\pi} \Gamma_{\text{MOS}}^2(t) G_{DS1}(t) R_p dt \approx 2\Gamma_{\text{rms}}^2 R_p \cdot G_{DS1EF} \quad (30)$$

where G_{DS1EF} is the effective drain-source conductance of one of the gm-devices expressed by

$$G_{DS1EF} = G_{DS1}[0] - G_{DS1}[2] \quad (31)$$

where $G_{DS1}[k]$ describes the k th Fourier coefficient of the instantaneous conductance, $G_{ds1}(t)$ [25]. F_{GM} can be calculated by

$$F_{GM} = \frac{1}{\pi} \int_0^{2\pi} \Gamma_{\text{MOS}}^2(t) \gamma G_{m1}(t) R_p dt \approx 2\Gamma_{\text{rms}}^2 \cdot \gamma \cdot R_p \cdot G_{M1EF} \quad (32)$$

Now, the effective negative transconductance of the oscillator needs to overcome the tank and its own channel resistance losses and therefore the noise due to G_M also increases.

$$G_{M1EF} = \frac{1}{A} \left(\frac{1}{R_p} + G_{DS1EF} \right) \quad (33)$$

where A is the voltage gain of feedback path between the tank and MOS gate. By substituting (33) into (32)

$$F_{GM} = 2\Gamma_{\text{rms}}^2 \cdot \frac{\gamma}{A} \cdot (1 + R_p G_{DS1EF}) \quad (34)$$

Consequently, the effective noise factor of the oscillator is given by

$$F = 2\Gamma_{\text{rms}}^2 \cdot \left(1 + \frac{\gamma}{A} \right) \cdot (1 + R_p G_{DS1EF}) \quad (35)$$

This is a general result and applicable to the class-B, C and F. The oscillator FoM normalizes the phase noise performance to the oscillation frequency and power consumption, yielding

$$FoM = -10 \log_{10} \left(\frac{10^3 K_B T}{2Q_t^2 \alpha_I \alpha_V} 2\Gamma_{\text{rms}}^2 \times \left(1 + \frac{\gamma}{A} \right) (1 + R_p G_{DS1EF}) \right) \quad (36)$$

where α_V is the voltage efficiency, defined as V_p/V_{DD} . To get a better insight, the circuit-to-phase noise mechanism, relative phase noise and power efficiency of different oscillator

TABLE II
COMPARISON OF DIFFERENT OSCILLATOR'S CLASSES FOR THE SAME V_{DD} (1.2 V), TANK Q-FACTOR (15), R_P (I.E., 220 Ω), AND CARRIER FREQUENCY (7 GHz) AT 3 MHz OFFSET FREQUENCY

| | Theoretical expression | Class-B | Dynamic biased Class-C | Class-F |
|-------------|---|------------------------------|--------------------------------|----------------------------|
| F_{RP} | $2\Gamma_{rms}^2 = \frac{1+9\zeta^2}{(1+3\zeta)^2}$ | 1 (average) | 1 (average) | 0.7 (best) |
| F_{GDS} | $2\Gamma_{rms}^2 R_P G_{DS1EF1}$ | 0.56 (worst) | 0.07 (best) | 0.27 (average) |
| F_{GM} | $2\Gamma_{rms}^2 \frac{\gamma}{A} (1 + R_P G_{DS1EF})$ | 1.56 γ = 2.02 (worst) | 1.07 γ = 1.39 (average) | 0.7 γ = 0.91 (best) |
| F (dB) | $10 \log_{10} (2 \Gamma_{rms}^2 \frac{\gamma}{A} (1 + \frac{\gamma}{A}) (1 + R_P G_{DS1EF}))$ | 5.5 (worst) | 3.9 (average) | 2.8 (best) |
| α_I | I_{H1}/I_B | 0.55 (worst) | 0.9 (best) | 0.63 (average) |
| α_V | V_P/V_{DD} | 0.8 (best) | 0.7 (average) | 0.8 (best) |
| PN (dBc/Hz) | $10 \log_{10} \left(\frac{K_B T R_P}{2 Q_0^2 V_P^2} \cdot F \cdot \left(\frac{\omega_0}{\Delta\omega} \right)^2 \right)$ | -133.5 (worst) | -134 (average) | -136 (best) |
| FoM (dB) | $-10 \log_{10} \left(\frac{10^3 K_B T}{2 Q_0^2 \alpha_I \alpha_V} 2\Gamma_{rms}^2 \frac{\gamma}{A} (1 + \frac{\gamma}{A}) (1 + R_P G_{DS1EF}) \right)$ | 191.2 (worst) | 194.5 (best) | 194.2 (\approx best) |

classes are also investigated and compared together in this section. Fig. 16(a)-(f) shows the oscillation voltage and drain current for the traditional, class-C and the proposed class-F oscillators for the same V_{DD} (i.e., 1.2 V), tank Q-factor (i.e., 15) and R_P (i.e., 220 Ω).

The α_V must be around 0.8 for the class B and F oscillators due to the voltage drop V_{dsat} across tail transistor needed to keep it in saturation. The combination of the tail capacitance and entering the gm-devices into the linear region reduces α_I of class-B from the theoretical value of $2/\pi$ to around 0.55. Fortunately, α_I is maintained around $2/\pi$ for class-F due to the pseudo-square drain voltage and larger gate amplitude. The class-C oscillator with a dynamic bias of the active transistor offers significant improvements over the traditional class-C, and maximizes the oscillation amplitude without compromising the robustness of the oscillator start-up [26]. Nevertheless, its α_V is around 0.7 to avoid gm-devices entering the triode region. Class-C drain current composed of tall and narrow pulses results in α_I equal to 0.9 (ideally 1).

Obtaining the ISF function is the first step in the calculation of the oscillator's effective noise factor. The class-B/C ISF function is a sinusoid in quadrature with the tank voltage [7], [27]. However, finding the exact equation of class-F ISF is not possible, hence, we had to resort to painstakingly long CadenceTM simulations to obtain the ISF curves. Fig. 16(g) shows the simulated class-F tank equivalent ISF function, which is smaller than the other classes for almost the entire oscillation period.

Fig. 16(h) demonstrates the tank effective noise factor along the oscillation period for different oscillator classes. The F_{RP} is 32% lower for the proposed class-F due to its special ISF properties. The gm-device M_1 channel conductance across the oscillation period is shown in Fig. 16(i). As expected, $G_{DS1}(t)$ of class-F exhibits the largest peak due to high oscillation swing at the gate and, consequently, injects more noise than other structures to the tank. On the other hand, class-C operates only in the saturation region and its effective transistor conductance is negligible. Fig. 16(j) stronger emphasizes that the gm-device resistive channel noise could even be 7 times higher than the tank noise when the M_1 operates in the linear region. To get a better insight, one need to simultaneously focus on Figs. 16(j) and (k). Although the class-F G_{DS1} generates lots of noise in the second half of the period, its relevant ISF value is very small there. Hence, the excessive transistor channel noise cannot convert to the phase noise and as shown in Fig. 16(l), the F_{GDS} of class-F is one half of the traditional oscillator. The transconductance loop gain of the different oscillator structures

are shown in Fig. 16(m). Class-F needs to exhibit the highest effective transconductance loop gain to compensate its larger gm-devices channel resistance losses. However, half of the required loop gain is covered by the transformer-based tank voltage gain. Fig. 16(o) demonstrates the active device effective noise factor along the oscillation period. Class-F offers the lowest F_{GM} due to its special ISF nature and the passive voltage gain between the tank and gate of the gm-transistors.

Table II summarizes the performance of different oscillator classes of this example. It can be concluded that class-F oscillator achieves the lowest circuit-to-phase noise conversion along the best phase noise performance with almost the same power efficiency as the class-C oscillator.

The use of transformer in the Class-F configuration offers an additional reduction of the $1/f^3$ phase noise corner. The transformer inherently rejects the common-mode signals. Hence, the $1/f$ noise of the tail current source can appear at the transformer's primary but it will be effectively filtered out on the path to the secondary winding. Consequently, the AM-to-PM conversion at the C_2 switched capacitors is entirely avoided.

Another $1/f$ noise upconversion mechanism is called the Groszkowski effect [28]. Groszkowski demonstrated that the presence of harmonic components of the active device current in the tank can cause a frequency drift from the tank resonance [29]. The harmonic components of the drain current mainly take the capacitance path due its lower impedance. As a consequence, the oscillation frequency must shift down to satisfy the resonance condition. Consequently, any variation in harmonic-to-fundamental drain current value due to the $1/f$ noise of M_T can modulate Groszkowski's frequency shift and show itself as a low frequency noise in the phase noise sidebands [29]. The class-F tank has fortunately two impedance peaks at the fundamental oscillation frequency and its 3rd harmonic. Hence, the 3rd harmonic component (i.e., the strongest among the higher harmonics) of drain current flows to the resistive part of the tank and does not contribute to Groszkowski's frequency shift. It effectively reduces the $1/f$ noise upconversion to the $1/f^3$ phase noise due to Groszkowski phenomenon.

C. Class-F Operation Robustness

Fig. 17(a) illustrates the tank input impedance magnitude and phase for the imperfect position of the second resonance frequency ω_2 . A 6% mismatch is applied to the C_2/C_1 ratio, which shifts ω_2 to frequencies higher than $3\omega_1$. Hence, the 3rd harmonic of the drain current is multiplied by a lower impedance

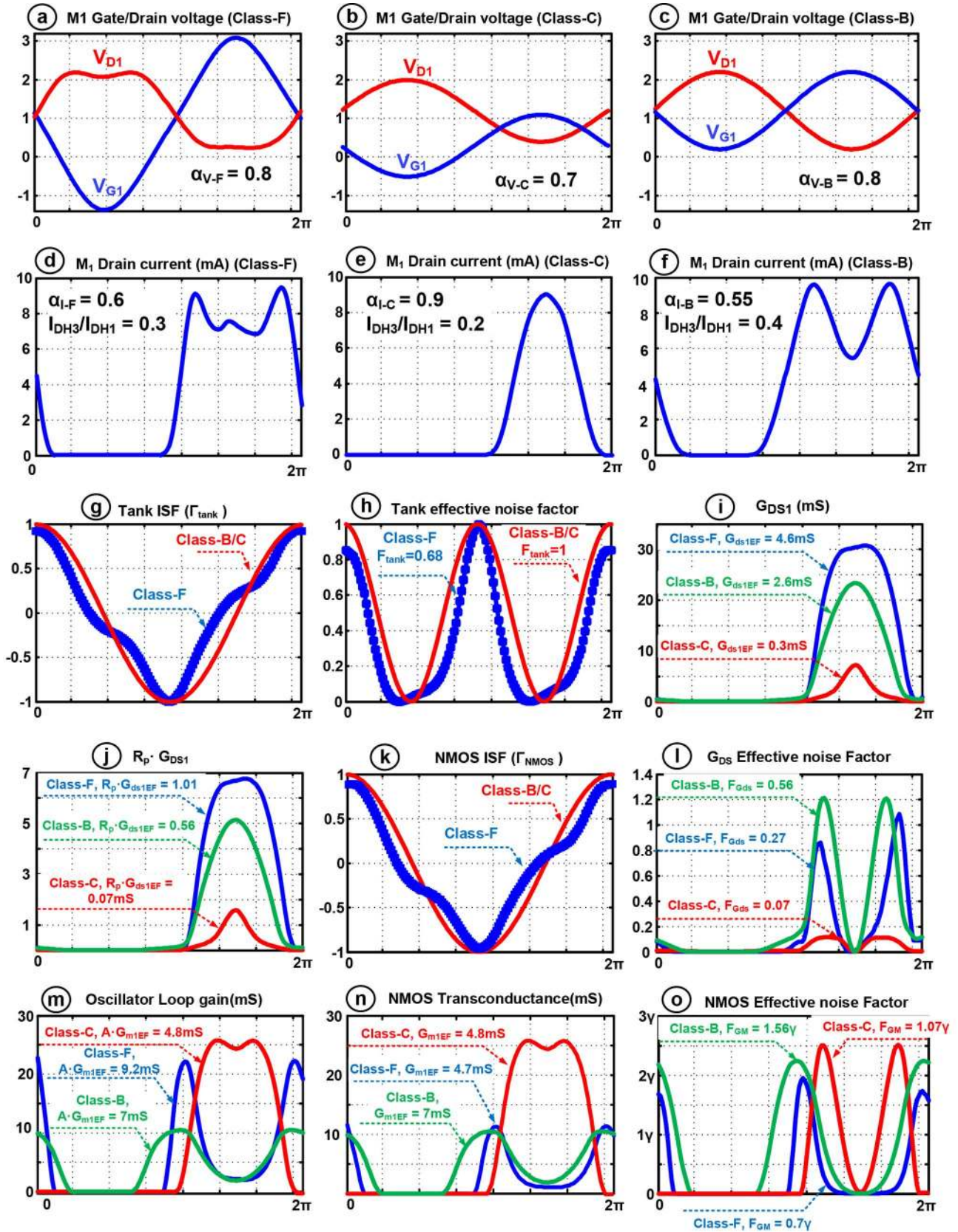


Fig. 16. Mechanisms of circuit noise to phase noise conversion in different classes of RF CMOS oscillator.

magnitude with a phase shift resulting in a distorted pseudo-square oscillation waveform as shown in Fig. 17(b). Intuitively, if the Q-factor at ω_2 was smaller, the tank impedance bandwidth around it would be wider. Therefore, the tank input impedance

phase shift and magnitude reduction would be less for a given ω_2 drift from $3\omega_1$. As a consequence, the oscillator would be less sensitive to the position of ω_2 and thus the tuning capacitance ratio. Based on the open-loop Q-factor analysis, substi-

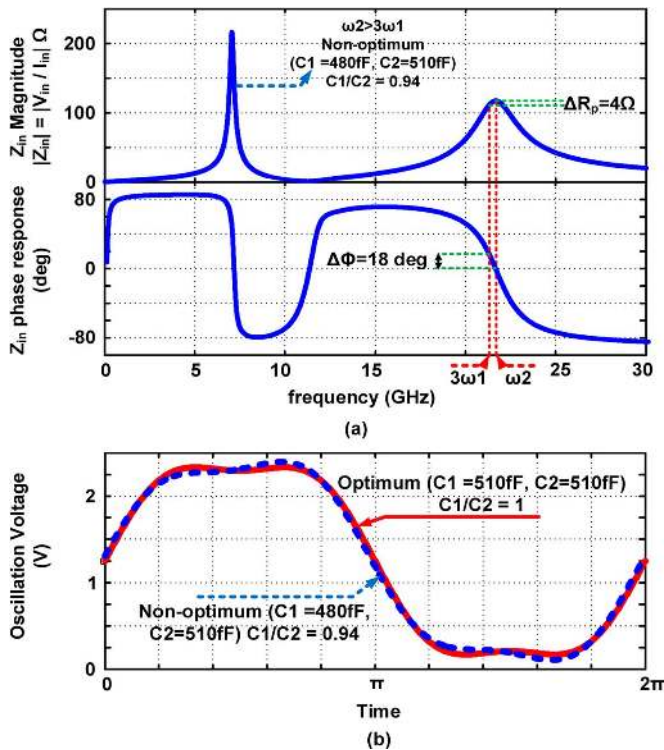


Fig. 17. Sensitivity of class-F oscillator to the position of the second resonant frequency: tank's input impedance magnitude and phase (top), oscillation waveform (bottom).

tuning $\omega^2 \approx 9/(L_s C_2 + L_p C_1)$ into (20), the Q_i is obtained as $0.3Q_0$ at ω_2 . Fortunately enough, the proposed tank configuration automatically reduces the equivalent tank Q-factor at ω_2 to 30% of the main resonance Q-factor. This is completely in line with the desire to reduce the sensitivity to the position of ω_2 in class-F. Consequently, a realistic example ± 30 fF variation in C_1 from its optimum point has absolutely no major side effects on the oscillator waveform and thus its phase noise performance, as apparent from Fig. 17. It is strongly emphasized that the circuit oscillates based on ω_1 resonance and low Q-factor at ω_2 has no adverse consequence on the oscillator phase noise performance.

IV. EXPERIMENTAL RESULTS

A. Implementation Details

The class-F oscillator, whose schematic was shown in Fig. 10(a), has been realized in TSMC 1P7M 65-nm CMOS technology with Alucap layer. The differential transistors are thick-oxide devices of $12(4\text{-}\mu\text{m}/0.28\text{-}\mu\text{m})$ dimension to withstand large gate voltage swing. However, the tail current source M_T is implemented as a thin-oxide $500\text{-}\mu\text{m}/0.24\text{-}\mu\text{m}$ device biased in saturation. The large channel length is selected to minimize its $1/f$ noise. Its large drain-bulk and drain-gate parasitic capacitances combined with $C_T = 2$ pF MOM capacitor shunt the M_T thermal noise to ground. The step-up 1:2 transformer is realized by stacking the $1.45\text{ }\mu\text{m}$ Alucap layer on top of the $3.4\text{ }\mu\text{m}$ thick top (M7 layer) copper metal. Its primary and secondary differential self-inductances are about 500 pH and 1500 pH, respectively, with the magnetic coupling

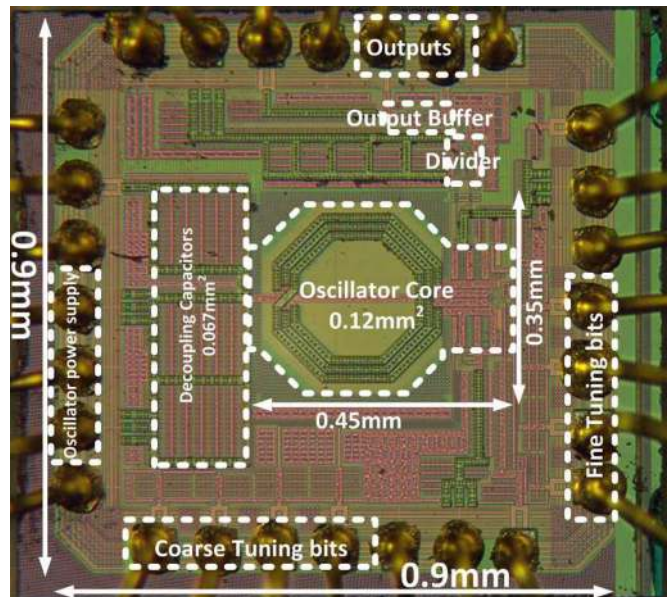


Fig. 18. Die photograph of class-F oscillator.

factor of 0.73. The transformer was designed with a goal of maximizing Q-factor of the secondary winding, Q_s , at the desired operating frequency. Based on (21), Q_s is the dominant factor in the tank equivalent Q-factor expression, provided $(L_s C_2)/(L_p C_1)$ is larger than one, which is valid for this oscillator prototype. In addition, the oscillation voltage is sinusoidal across the secondary winding. It means the oscillator phase noise is more sensitive to the circuit noise at the secondary winding compared to the primary side with the pseudo-square waveform. Four switched MOM capacitors $B_{C0} - B_{C3}$ placed across the secondary winding realize coarse tuning bits, while the fine control bits $B_{F0} - B_{F3}$ with LSB size of 20 fF adjust the position of ω_2 near $3\omega_1$. The center tap of the secondary winding is connected to the bias voltage, which is fixed around 1 V to guarantee safe oscillator start-up in all process corners. A resistive shunt buffer interfaces the oscillator output to the dynamic divider [2]. A differential output buffer drives a 50- Ω load. The separation of the oscillator core and divider/output buffer voltage supplies and grounds serves to maximize the isolation between the circuit blocks. The die micrograph is shown in Fig. 18. The oscillator core die area is 0.12 mm^2 .

B. Measurement Results

The measured phase noise at 3.7 GHz (after the on-chip $\div 2$ divider) at 1.25 V and 12 mA current consumption is shown in Fig. 19. The phase noise of -142.2 dBc/Hz at 3 MHz offset lies on the 20 dB/dec slope, which extrapolates to -158.7 dBc/Hz at 20 MHz offset (-170.8 dBc/Hz when normalized to 915 MHz) and meets the GSM TX mobile station (MS) specification with a very wide 8 dB margin. The oscillation purity of the class-F oscillator is good enough to compare its performance to cellular basestation (BTS) phase noise requirements. The GSM/DCS "Micro" BTS phase noise requirements are easily met. However, the phase noise would be off by 3 dB for the toughest DCS-1800 "Normal" BTS specification at 800 kHz offset frequency [30]. The $1/f^3$ phase noise corner is around 700 kHz at

TABLE III
COMPARISON OF STATE-OF-THE-ART OSCILLATORS

| | This Work | [9] | [8] | [30] | [10] | [31] | [2] | [19] |
|---|-----------|---------|-----------------|------------------|-----------|--------------|-------------|-----------|
| Technology | 65nm | 130nm | 350 μ m | 65nm | 55nm | BiCMOS 130nm | 90nm | 65nm |
| Supply voltage (V) | 1.25 | 1 | 2.5 | 1.2 | 1.5 | 3.3 | 1.4 | 0.6 |
| Frequency (GHz) | 3.7 | 5.2 | 1.2 | 3.92 | 3.35 | 1.56 | 0.915 | 3.7 |
| Tuning range (%) | 25 | 14 | 18 | 10.2 | 31.4 | 9.6 | 24.3 | 77 |
| Phase noise at 3 MHz (dBc/Hz) | -142.2 | -141.2 | -152 | -141.7 | -142 | -150.4 | -149 | -137.1 |
| Norm. phase noise ¹ (dBc/Hz) | -154.3 | -147.5 | -154.8 | -154.4 | -153.3 | -155 | -149 | -149.21 |
| Power consumption (mW) | 15 | 1.4 | 9.25 | 25.2 | 27 | 290 | 25.2 | 10.5 |
| FoM (dB) | 192.2 | 195 | 195 | 189.9 | 189 | 180 | 184.6 | 188.7 |
| $F_oM_T^2$ (dB) | 200.2 | 198.4 | 200.7 | 190 | 199 | 179.7 | 192.3 | 206.5 |
| Number of inductors & transformers | 1 | 1 | 2 | 2 | 1 | 1 | 1 | 1 |
| Oscillator structure | Class F | Class C | Noise Filtering | Clip-and-Restore | Class B/C | Colpitts | Traditional | Dual mode |

¹ phase noise at 3 MHz offset frequency normalized to 915 MHz carrier.
² $F_oM_T = |PN| + 20 \log_{10}((f_0/\Delta f) (TR/10)) - 10 \log_{10}(P_{DC}/1mW)$

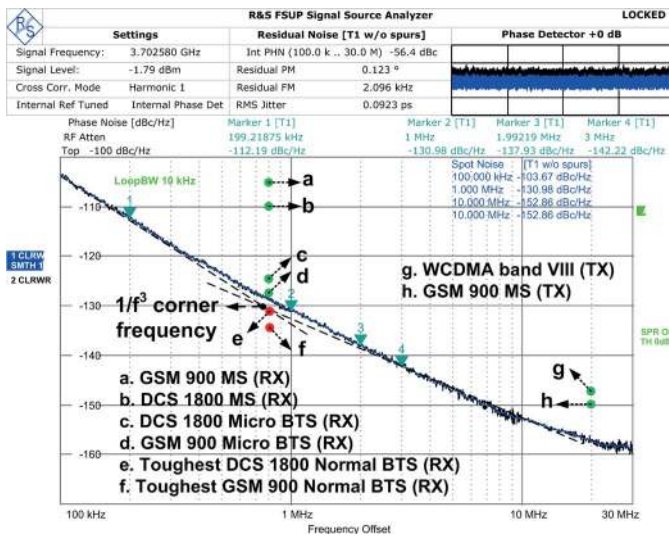


Fig. 19. Measured phase noise at 3.7 GHz and power dissipation of 15 mW. Specifications (MS: mobile station, BTS: basestation) are normalized to the carrier frequency.

the highest frequency due to the asymmetric layout of the oscillator differential nodes further magnified by the dominance of parasitics in the equivalent tank capacitance. The $1/f^3$ phase noise corner moves to around 300 kHz at the middle and low part of the tuning range. The noise floor is -160 dBc/Hz and dominated by thermal noise from the divider and buffers. The oscillator has a 25% tuning range, from 5.9 to 7.6 GHz. Fig. 20 shows the average phase noise performance of four samples at 3 MHz offset frequency across the tuning range (after the divider), together with the corresponding FoM. The average FoM is as high as 192 dBc/Hz and varies about 2 dB across the tuning range. The divided output frequency versus supply is shown in Fig. 21 and reveals very low frequency pushing of 50 MHz/V and 18 MHz/V at the highest and lowest frequencies, respectively.

The phase noise of the class-F oscillator was measured at the fixed frequency of 3.5 GHz for two configurations. In the first configuration, the C_2/C_1 ratio was set to one to align the second resonant frequency ω_2 exactly at the 3rd harmonic of the fundamental frequency ω_1 . This is the optimum configuration of the class-F oscillator (Fig. 22, top). In the second con-

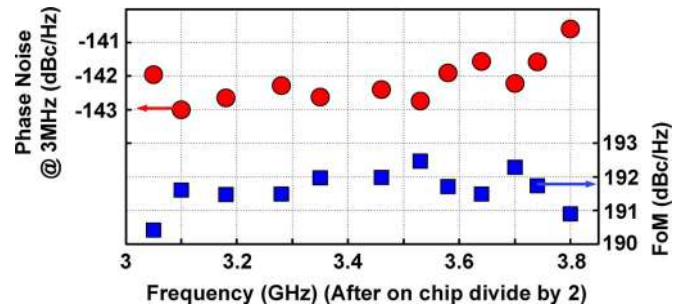


Fig. 20. Phase noise and figure-of-merit (FoM) at 3 MHz offset versus carrier frequency.

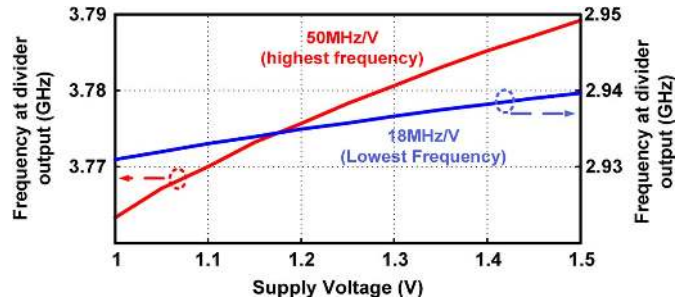


Fig. 21. Frequency pushing due to supply voltage variation.

figuration, the oscillation frequency is kept fixed but an unrealistically high 40% mismatch was applied to the C_2/C_1 ratio, which lowers ω_2 , in order to see its effects on the phase noise performance (see Fig. 22, bottom). As a consequence, the 3rd harmonic component of the drain oscillation voltage is reduced and a phase shift can be seen between voltage waveform components at $3\omega_1$ and ω_1 . Therefore, its ISF rms value is worse than optimum, thus causing a 2 dB phase noise degradation in the 20 dB/dec region. In addition, the voltage waveform demonstrates more asymmetry in the rise and fall times, which translates to the non-zero ISF dc value and increases the upconversion factor of the $1/f^3$ phase noise corner of gm-devices. As can be seen in Fig. 22, the $1/f^3$ phase noise corner is increased by 25% or 100 kHz in the non-optimum case. It results in a 3 dB phase noise penalty in the flicker noise region.

Table III summarizes performance of the proposed class-F oscillator and compares it with the relevant state-of-the-art. The

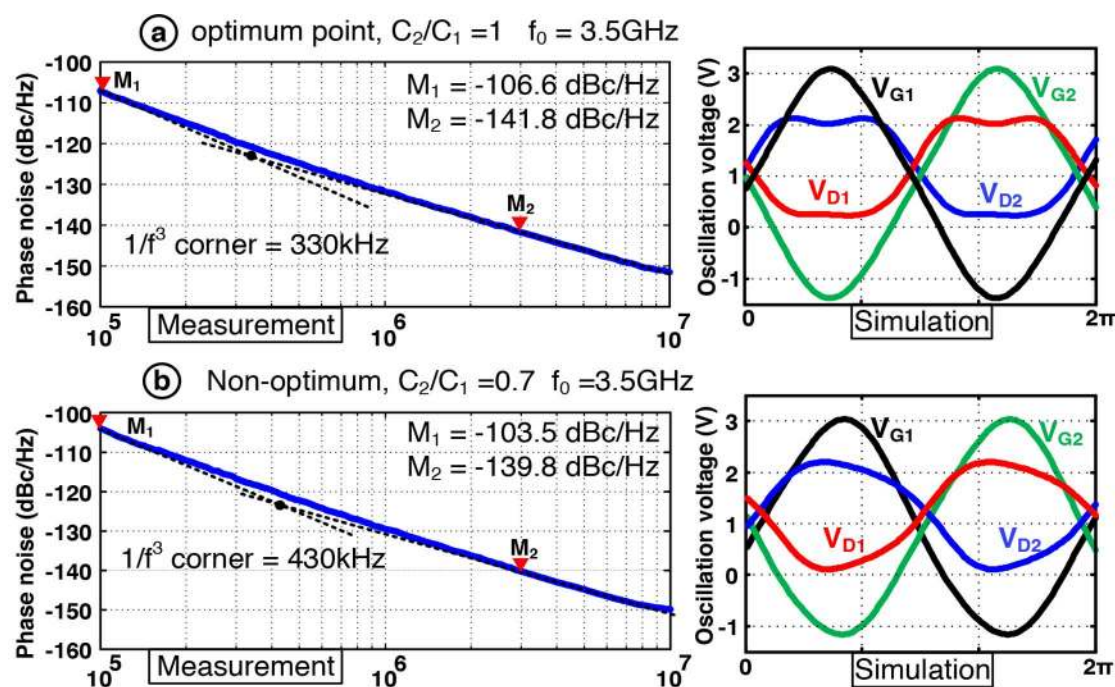


Fig. 22. Measured phase noise at 3.5 GHz and simulated oscillation waveforms: (a) optimum case; (b) exaggerated non-optimum case.

class-F demonstrates a 5 dB phase noise and 7 dB FoM improvements over the traditional commercial oscillator [2] with almost the same tuning range. For the same phase noise performance range (-154 to -155 dBc/Hz) at 3 MHz offset for the normalized 915 MHz carrier, the class-F oscillator consumes only 15 mW, which is much lower than with Colpitts [31], class B/C [10], and clip-and-restore [30] topologies. Only the noise-filtering-technique oscillator [8] offers a better power efficiency but at the cost of an extra dedicated inductor and thus larger die. Also, it uses a 2.5 V supply thus making it unrealistic in today's scaled CMOS. From the FoM point of view, the class-C oscillator [9] exhibits a better performance than the class-F oscillator. However, the voltage swing constraint in class-C limits its phase noise performance. As can be seen, the class-F demonstrates more than 6 dB better phase noise with almost the same supply voltage. Consequently, the class-F oscillator has reached the best phase noise performance with the highest power efficiency at low voltage supply without the die area penalty of the noise-filtering technique or voltage swing constraint of the class-C VCOs.

V. CONCLUSION

We have proposed a new structure for LC-tank oscillators that introduces an impedance peak around the third harmonic of the oscillating waveform such that the third harmonic of the active device current converts into voltage and, together with the fundamental component, creates a pseudo-square oscillation voltage. The additional peak of the tank impedance is realized with a transformer-based resonator. As a result, the oscillator impulse sensitivity function reduces thus lowering the conversion sensitivity of phase noise to various noise sources, whose mechanisms are analyzed in depth. Chief of these mechanisms arises when the active gm-devices periodically enter the triode

region during which the LC-tank is heavily loaded while its equivalent quality factor is significantly reduced. The voltage gain, relative pole position, impedance magnitude and equivalent quality factor of the transformer-based resonator are quantified at its two resonant frequencies. The gained insight reveals that the secondary to the primary voltage gain of the transformer can be even larger than its turns ratio. A comprehensive study of circuit-to-phase-noise conversion mechanisms of different oscillators' structures shows the proposed class-F exhibits the lowest phase noise at the same tank's quality factor and supply voltage. Based on this analysis, a class-F oscillator was prototyped in 65-nm CMOS technology. The measurement results prove that the proposed oscillator can achieve a state-of-the-art phase noise performance with the highest power efficiency at low voltage power supply without die area penalty or voltage swing constraint.

ACKNOWLEDGMENT

The authors thank A. Akhnoukh, W. Straver, A. Kaichouhi, Morteza Alavi, Wanghua Wu, A. Visweswaran, A. Ahmadi Mehr, M. Tohidian, and I. Madadi for the measurement support and technical discussions.

REFERENCES

- [1] E. Hegazi and A. A. Abidi, "A 17-mW transmitter and frequency synthesizer for 900-MHz GSM fully integrated in 0.35- μ m CMOS," *IEEE J. Solid-State Circuits*, vol. 38, no. 5, pp. 782–792, May 2003.
- [2] R. B. Staszewski *et al.*, "All-digital PLL and transmitter for mobile phones," *IEEE J. Solid-State Circuits*, vol. 40, no. 12, pp. 2469–2482, Dec. 2005.
- [3] L. Vercesi, L. Fanori, F. D. Bernardinis, A. Liscidini, and R. Castello, "A dither-less all digital PLL for cellular transmitters," *IEEE J. Solid-State Circuits*, vol. 47, no. 8, pp. 1908–1920, Aug. 2012.
- [4] H. Darabi *et al.*, "A quad-band GSM/GPRS/EDGE SoC in 65 nm CMOS," *IEEE J. Solid-State Circuits*, vol. 46, no. 4, pp. 870–882, Apr. 2011.

- [5] J. Borremans *et al.*, "A 40 nm CMOS 0.4–6 GHz receiver resilient to out-of-band blockers," *IEEE J. Solid-State Circuits*, vol. 46, no. 7, pp. 1659–1671, Jul. 2011.
- [6] J. Rael and A. Abidi, "Physical processes of phase noise in differential LC oscillators," in *Proc. IEEE Custom Integr. Circuits Conf.*, Sep. 2000, pp. 569–572.
- [7] P. Andreani, X. Wang, L. Vandi, and A. Fard, "A study of phase noise in Colpitts and LC-tank CMOS oscillators," *IEEE J. Solid-State Circuits*, vol. 40, no. 5, pp. 1107–1118, May 2005.
- [8] E. Hegazi, H. Sjolund, and A. A. Abidi, "A filtering technique to lower LC oscillator phase noise," *IEEE J. Solid-State Circuits*, vol. 36, no. 12, pp. 1921–1930, Dec. 2001.
- [9] A. Mazzanti and P. Andreani, "Class-C harmonic CMOS VCOs, with a general result on phase noise," *IEEE J. Solid-State Circuits*, vol. 43, no. 12, pp. 2716–2729, Dec. 2008.
- [10] L. Fanori, A. Liscidini, and P. Andreani, "A 6.7-to-9.2 GHz 55 nm CMOS hybrid class-B/class-C cellular TX VCO," in *IEEE Int. Solid-State Circuits Conf. (ISSCC) Dig. Tech. Papers*, Feb. 2012, pp. 354–355.
- [11] H. Kim, S. Ryu, Y. Chung, J. Choi, and B. Kim, "A low phase-noise CMOS VCO with harmonic tuned LC tank," *IEEE Trans. Microw. Theory Tech.*, vol. 54, no. 7, pp. 2917–2923, Jul. 2006.
- [12] M. Babaie and R. B. Staszewski, "Third-harmonic injection technique applied to a 5.87–to-7.56 GHz 65 nm class-F oscillator with 192 dBc/Hz FoM," in *IEEE Int. Solid-State Circuits Conf. (ISSCC) Dig. Tech. Papers*, Feb. 2013, pp. 348–349.
- [13] A. Hajimiri and T. H. Lee, "A general theory of phase noise in electrical oscillators," *IEEE J. Solid-State Circuits*, vol. 33, no. 2, pp. 179–194, Feb. 1998.
- [14] B. Razavi, "A millimeter-wave circuit technique," *IEEE J. Solid-State Circuits*, vol. 43, no. 9, pp. 2090–2098, Sep. 2008.
- [15] J. R. Long, "Monolithic transformers for silicon RF IC design," *IEEE J. Solid-State Circuits*, vol. 35, no. 9, pp. 1368–1382, Sep. 2000.
- [16] A. Bevilacqua, F. P. Pavan, C. Sandner, A. Gerosa, and A. Neviani, "Transformer-based dual-mode voltage-controlled oscillators," *IEEE Trans. Circuits Syst. II, Exp. Briefs*, vol. 54, no. 4, pp. 293–297, Apr. 2007.
- [17] A. Goel and H. Hashemi, "Frequency switching in dual-resonance oscillators," *IEEE J. Solid-State Circuits*, vol. 42, no. 3, pp. 571–582, Mar. 2007.
- [18] B. Razavi, "Cognitive radio design challenges and techniques," *IEEE J. Solid-State Circuits*, vol. 45, no. 8, pp. 1542–1553, Aug. 2010.
- [19] G. Li, L. Liu, Y. Tang, and E. Afshari, "A low-phase-noise wide-tuning-range oscillator based on resonant mode switching," *IEEE J. Solid-State Circuits*, vol. 47, no. 6, pp. 1295–1308, Jun. 2012.
- [20] R. Degraeve *et al.*, "A new model for the field dependence of intrinsic and extrinsic time-dependent dielectric breakdown," *IEEE Trans. Electron Devices*, vol. 45, no. 2, pp. 472–481, Feb. 1998.
- [21] M. Babaie and R. B. Staszewski, "A study of RF oscillator reliability in nanoscale CMOS," in *Proc. IEEE 21st European Conf. Circuit Theory and Design (ECCTD)*, Sep. 2013.
- [22] B. Razavi, "A study of phase noise in CMOS oscillators," *IEEE J. Solid-State Circuits*, vol. 31, no. 3, pp. 331–343, Mar. 1996.
- [23] H. Krishnaswamy and H. Hashemi, "Inductor and transformer-based integrated RF oscillators: A comparative study," in *Proc. IEEE Custom Integr. Circuits Conf.*, Sep. 2006, pp. 381–384.
- [24] P. Andreani and J. R. Long, "Misconception regarding of transformer resonators in monolithic oscillator," *Electronic Lett.*, vol. 42, no. 7, Mar. 2006.
- [25] D. Murphy, J. J. Rael, and A. A. Abidi, "Phase noise in LC oscillators: A phasor-based analysis of a general result and of loaded," *IEEE Trans. Circuits Syst. I, Reg. Papers*, vol. 57, no. 6, pp. 1187–1203, Jun. 2010.
- [26] L. Fanori and P. Andreani, "Low-phase-noise 3.4–4.5 GHz dynamic bias class-C CMOS VCOs with a FoM of 191 dBc/Hz," in *Proc. Eur. Solid State Circuits Conf.*, Sep. 2012, pp. 406–409.
- [27] P. Andreani and A. Fard, "More on the phase noise performance of CMOS differential-pair LC-tank oscillators," *IEEE J. Solid-State Circuits*, vol. 41, no. 12, pp. 2703–2712, Dec. 2006.
- [28] J. Groszkowski, "The impedance of frequency variation and harmonic content, and the problem of constant-frequency oscillator," *Proc. IRE*, vol. 21, pp. 958–981, 1933.
- [29] A. Bevilacqua and P. Andreani, "An analysis of 1/f noise to phase noise conversion in CMOS harmonic oscillators," *IEEE Trans. Circuits Syst. I, Reg. Papers*, vol. 59, no. 5, pp. 938–945, May 2012.
- [30] A. Visweswaran, R. B. Staszewski, and J. R. Long, "A clip-and-restore technique for phase desensitization in a 1.2 V 65 nm CMOS oscillator for cellular mobile and base stations," in *IEEE Int. Solid-State Circuits Conf. (ISSCC) Dig. Tech. Papers*, Feb. 2012, pp. 350–351.
- [31] J. Steinkamp *et al.*, "A Colpitts oscillator design for a GSM base station synthesizer," in *IEEE Radio Frequency Integrated Circuits Symp.*, Jun. 2007, pp. 405–408.



Masoud Babaie (S'12) received the B.Sc. degree (with highest honors) from Amirkabir University of Technology (Tehran Polytechnic), Tehran, Iran, in 2004, and the M.Sc. degree from Sharif University of Technology, Tehran, Iran, in 2006, both in electrical engineering.

He joined Kavoshcom R&D group in Tehran, Iran, in 2006 where he was involved in designing tactical communication systems. He was appointed the CTO of the company between 2009 and 2011.

He is currently working toward the Ph.D. degree at the Delft University of Technology, The Netherlands. His research interests include analog and RF IC design for wireless communications.



Robert Bogdan Staszewski (F'09) received the B.S.E.E. (*summa cum laude*), M.S.E.E., and Ph.D. degrees from the University of Texas at Dallas in 1991, 1992, and 2002, respectively.

From 1991 to 1995 he was with Alcatel Network Systems in Richardson, TX, USA, working on SONET cross-connect systems for fiber optics communications. He joined Texas Instruments in Dallas, TX, USA, in 1995 where he was elected Distinguished Member of Technical Staff. Between 1995 and 1999, he was engaged in advanced CMOS

read channel development for hard disk drives. In 1999, he co-started a Digital RF Processor (DRP™) group within Texas Instruments with a mission to invent new digitally intensive approaches to traditional RF functions for integrated radios in deeply-scaled CMOS processes. He was appointed a CTO of the DRP group between 2007 and 2009. In July 2009 he joined Delft University of Technology in The Netherlands, where he is a Professor. He has authored and co-authored one book, three book chapters, 150 journal and conference publications, and holds 110 issued US patents. His research interests include nanoscale CMOS architectures and circuits for frequency synthesizers, transmitters and receivers.

Prof. Staszewski has been a TPC member of ISSCC, RFIC, ESSCIRC, and RFIT. He is an IEEE Fellow and a recipient of IEEE Circuits and Systems Industrial Pioneer Award.